Hindawi
Active and Passive Electronic Components
Volume 2019, Article ID 1584724, 18 pages
https://doi.org/10.1155/2019/1584724

Research Article

Full-Phase Operation Transresistance-Mode Precision Full-Wave Rectifier Designs Using Single Operational Transresistance Amplifier

Hung-Chun Chien

Department of Electronic Engineering, Ming Chuan University, No. 5, Deming Road, Guishan District, Taoyuan City 333, Taiwan

Correspondence should be addressed to Hung-Chun Chien; hcchien@mail.mcu.edu.tw

Received 7 November 2018; Revised 20 January 2019; Accepted 6 February 2019; Published 3 March 2019

Academic Editor: Stephan Gift

This study proposed the designs of two full-phase operation transresistance-mode (TRM) precision full-wave rectifiers. The first circuit consisted of a single operational transresistance amplifier (OTRA), four diodes, and a resistor. The second scheme was an OTRA combined with a full metal-oxide semiconductor field-effect transistor-based design, which is preferable for integrated circuit implementation because no passive components are used in the circuit topology. Based on our literature review, this is the first study that discussed a full-phase operation transresistance-mode precision full-wave rectifier consisting of a single OTRA and few passive components. In this paper, several previously reported precision full-wave rectifiers consisting of various active devices are first reviewed followed by the proposed OTRA-based transresistance-mode precision full-wave rectifiers and an analysis of nonideal effects. Furthermore, computer simulations and experimental results are presented to verify the validity of the proposed circuits, which were consistent with the theoretical predictions.

1. Introduction

Rectification circuits have numerous electronic and electrical applications, including communication systems, power conversion circuits, instrument and measurement equipment, and sensor interfaces. Typically, passive-type rectification circuits can be easily constructed using diodes. However, the passive-type rectifiers cannot function accurately when the incoming signal has an amplitude lower than the threshold voltage of the diodes. To process low-level signals for rectification, precision rectifiers (also called active-type rectifiers) must be used. Conventional precision rectifiers were constructed using operational amplifiers (OAs) [1]. However, OA-based precision rectifiers operate efficiently only at low frequencies. Thus, the realization of high-performance and versatile precision rectifiers is one of the crucial research topics in the current analog signal processing circuit design research area. According to our review of relevant literature, several previous studies have explored the realization of precision full-wave rectifiers by employing second-generation current conveyors (CCIIs) [2–5]. These contributions have sparked great interest among many researchers to explore various high-performance precision rectifiers until now. In addition to these early reports [2–5], another possible design for implementing a voltage-mode (VM) CCII-based full-wave rectifier was reported [6]. In 2006, the CCII-based resistorless full-wave rectifier was introduced by employing two CCIIs and three n-channel metal-oxide semiconductor field-effect transistors (MOSFETs) [7]. To reduce the number of active devices used, an improved version based on a dual-X CCII (DXCCII) and three n-channel MOSFETs was subsequently presented [8]. In addition to CCII-based designs, previous studies have focused on using operational transconductance amplifiers (OTAs) to create precision rectifiers. In 1989, a possible design for implementing a voltage-mode (VM) OTA-based precision half-wave rectifier can be found in [9]. A VM full-wave rectifier composed of one fully differential input and output operational transconductance amplifier (FDIO-OTA), four diodes, and a resistor was reported in [10]. Other feasible circuit topologies for realizing OTA-based full-wave rectifiers were presented in [11]. Recently, an OTA-based current-mode (CM) full-wave rectifier was demonstrated [12]. The main advantage of these OTA-based solutions [10–12] is that the amplitude of the rectified output

Table 1: Comparisons among various precision full-wave rectifiers.

Reference	Type of active devices	Number of passive components	Rectifier output mode	Operation mode	Buffer circuit requirement	Highest operation frequency
[6]	2 CCIIs	3 resistors 2 diodes	Single-phase output rectification	Voltage mode	Yes	10 MHz
[7]	2 CCIIs 3 MOSFETs	------	Single-phase output rectification	Voltage mode	Yes	250 kHz
[8]	1 DXCCII 3 MOSFETs	------	Single-phase output rectification	Voltage mode	Yes	1 MHz
[10]	1 FDIO-OTA	1 resistor 4 diodes	Single-phase output rectification	Voltage mode	Yes	50 MHz
[11]	5 OTAs	2 resistors	Dual-phase output rectification	Voltage mode	Yes	10 kHz
[12]	1 OTA	2 resistors 2 diodes	Single-phase output rectification	Current mode	No	100 kHz
[12]	1 DVCC	3 resistors 2 diodes	Single-phase output rectification	Current mode	No	100 kHz
[13]	2 CDTAs 1 MO-CF	2 resistors 4 diodes	Single-phase output rectification	Current mode	No	1 MHz
[14]	1 CDTA	1 resistor 2 diodes	Single-phase output rectification	Current mode	No	5 MHz
[15]	1 MZC-CDTA 2 MOSFETs	------	Single-phase output rectification	Current mode	No	10 kHz
[16]	1 CDTA	2 resistors 1 diode	Single-phase output rectification	Current mode	No	5 MHz
[17]	4 CCCIIs	6 resistors	Single-phase output rectification	Transconductance mode	No	100 kHz
[18]	1 CCCII 2 MOSFETs	2 resistors	Single-phase output rectification	Voltage mode	Yes	50 kHz
[19]	1 CCII 1 UVC	2 resistors 2 diodes	Dual-phase output rectification	Voltage mode	Yes	100 kHz
[20]	1 CCII 2 OPAs	3 resistors 2 diodes	Single-phase output rectification	Voltage mode	No	500 kHz
[21]	2 OTRAs 2 MOSFETs	3 resistors	Single-phase output rectification	Voltage mode	Yes	50 kHz
[22]	3 OTRAs 6 MOSFETs	8 resistors	Single-phase output rectification	Voltage mode	Yes	1 kHz
Proposed 1	1 OTRA	1 resistor 4 diodes	Dual-phase output rectification	Transresistance mode	No	5 MHz
Proposed 2	1 OTRA 6 MOSFETs	------	Dual-phase output rectification	Transresistance mode	No	5 MHz

signal can be tuned electronically by adjusting the bias current of the OTA. In the past several years, current differencing transconductance amplifier (CDTA)-based precision rectifiers have received a considerable amount of attention. In 2011, Tangsrirat et al. [13] proposed two CDTA-based CM full-wave rectifiers. The presented circuits were constructed using one multiple-output current follower, two CDTAs, four diodes, and two resistors. Three improved designs based on CDTA and a modified Z-copy current difference transconductance amplifier (MZC-CDTA) can also be found in the literature [14–16]. Two additional approaches presented full-wave rectifiers that employed a current-controlled current conveyor (CCCII) [17, 18]. Moreover, a CM circuit topology reported in [12] was designed using a differential voltage current conveyor (DVCC) and five passive components. In addition to the topologies for realizing precision rectifiers by adopting single-type active devices [2–18], previous studies have presented several schemes that combine diverse active devices, including the CCII, OA, and universal voltage conveyor (UVC) [19, 20]. Three recent studies demonstrating VM rectification solutions, which were designed by using operational transresistance amplifiers (OTRAs), have been reported in [21–23]. Although implementation of OTRA-based VM rectification circuits has been presented [21–23], the concept of the full-phase operation transresistance-mode (TRM) precision full-wave rectifier has not been discussed in previous studies. Therefore, this study proposed two compact circuit topologies to explore transresistance-mode precision rectification circuits. A quantitative comparison with existing full-wave rectifiers is presented in Table 1.

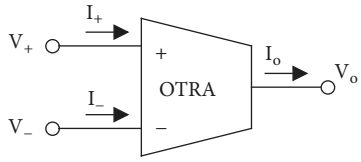

Figure 1: Circuit symbol of an OTRA.

The proposed circuits are characterized by the following features: (1) a tunable rectified output signal amplitude with dual-phase rectification output signal property in a single-circuit scheme; (2) a resistorless design (the second proposed topology), which has high potential in the integrated circuit manufacturing process; and (3) low-impedance output, which facilitates the use of cascading applications without the need for supplementary buffer circuits. The remainder of this paper is organized as follows. Section 2 presents the functional block and implementation of an OTRA followed by the operation principle of the proposed OTRA-based full-phase operation transresistance-mode precision full-wave rectifiers. Section 3 presents an analysis of the nonideal effects. Section 4 presents the computer simulations and experimental results to demonstrate the effectiveness of the proposed circuits. A conclusion is included in Section 5 to summarize this study.

2. Proposed Full-Phase Operation Transresistance-Mode Precision Full-Wave Rectifiers

An OTRA is a high-gain transimpedance-type active building block, which was first introduced in 1992 [24]. Figure 1 presents the circuit symbol of an OTRA, which is a three-terminal active device with two internal grounded current input terminals (I_+ and I_-) and a low-impedance voltage output terminal (V_o). The terminal relations of an OTRA are described in (1), which shows that the output voltage is produced by an inherent transresistance gain (R_m) multiplied by the difference of the input currents (I_+ and I_-). The transresistance gain (R_m) approaches infinity under an ideal scenario.

$$\begin{bmatrix} V_+ \\ V_- \\ V_o \end{bmatrix} = \begin{bmatrix} 0 & 0 & 0 \\ 0 & 0 & 0 \\ R_m & R_m & 0 \end{bmatrix} \begin{bmatrix} I_+ \\ I_- \\ I_o \end{bmatrix} \quad (1)$$

Figure 2(a) presents a CMOS transistor-level implementation of the OTRA [24]. In the circuit (Figure 2(a)), (M_1–M_{16}) simulates a current differencing circuit to generate current as the difference between I_+ and I_- currents. To generate the output voltage (V_o), which is a function of the transresistance gain (R_m) with respect to the difference between the I_+ and I_- currents, a voltage buffer (M_{17}–M_{22}) was applied. In addition to the CMOS realization presented in Figure 2(a), an OTRA can be easily implemented using commercially available integrated circuits (AD844s) in a configuration depicted in Figure 2(b) [25]. The circuit presented in Figure 2(b) can provide a viable method to fulfill the requirements of the experiments.

Figure 3 presents the circuit diagram and corresponding input and output transfer characteristics of the proposed full-phase operation transresistance-mode precision full-wave rectifier. The circuit is composed of a single OTRA, four diodes, and a resistor. Two diverse operating modes of the circuit (Figure 3(b)) are described as follows. In the circuit mode 1, the switch (S) must be arranged in a manner that a is connected to b. In the positive input current cycle ($I_{in} > 0$), diode D_3 is activated and diode D_4 is inactivated, thus causing the circuit to produce a positive-polarity rectified output signal at V_o. In the negative input current cycle ($I_{in} < 0$), diode D_3 is inactivated and diode D_4 is activated, resulting in a negative-polarity rectified output signal at V_o. Consequently, a positive full-wave rectification output can be obtained when the circuit is operated in mode 1. In a negative full-wave rectification output (mode 2) arrangement, the switch (S) must be arranged in a manner that a is connected to c. In the positive input current cycle ($I_{in} > 0$), D_1 is activated and D_2 is inactivated, resulting in a negative-polarity rectified output signal at V_o. Conversely, in the negative input current cycle ($I_{in} < 0$), D_1 is inactivated and D_2 is activated, resulting in a positive-polarity rectified output signal at V_o. Thus, a negative full-wave rectification output is obtainable through mode 2. A routine circuit analysis yielded the formulas for the input and output in two diverse full-wave rectification modes, which are expressed in (2) and (3), respectively. Equations (2) and (3) indicate that the circuit (Figure 3) performs the full-phase operation full-wave rectification function in a single-circuit scheme, and the amplitude of the rectified output signal can be tuned using the resistor R.

$$V_o \text{ (mode 1)} = \begin{cases} RI_{in} & (I_{in} > 0) \\ -RI_{in} & (I_{in} < 0) \end{cases} \quad (2)$$

$$V_o \text{ (mode 2)} = \begin{cases} -RI_{in} & (I_{in} > 0) \\ RI_{in} & (I_{in} < 0) \end{cases} \quad (3)$$

The circuit presented in Figure 4 is an extended design of the proposed circuit (Figure 3), which is a full MOSFET-based circuit topology. In Figure 4, the MOS transistors (M_A and M_B) function as active resistors, which are used to replace the resistor R in the circuit (Figure 3). The formula for the active resistor (M_A and M_B) is defined in (4) [26]. In (4), μ_n is the effective channel electronic mobility, C_{ox} is the gate-oxide capacitance per unit area, and W and L are the channel width and length, respectively, of M_A and M_B. Furthermore, in Figure 4, the MOS transistors (M_1–M_4) function as diodes (D_1–D_4) [9]. After applying (4) into (2) and (3), the formulas for the input and output in two diverse rectification modes are expressed in (5) and (6). The circuit (Figure 4) possesses the following features: (1) it is a resistorless scheme with a full MOSFET-based design and thus has high potential in the integration circuit manufacturing process; (2) it yields a low-output impedance at output V_o, which enables cascading application without supplementary buffer circuits; (3) a full-phase operation full-wave rectification function is achievable

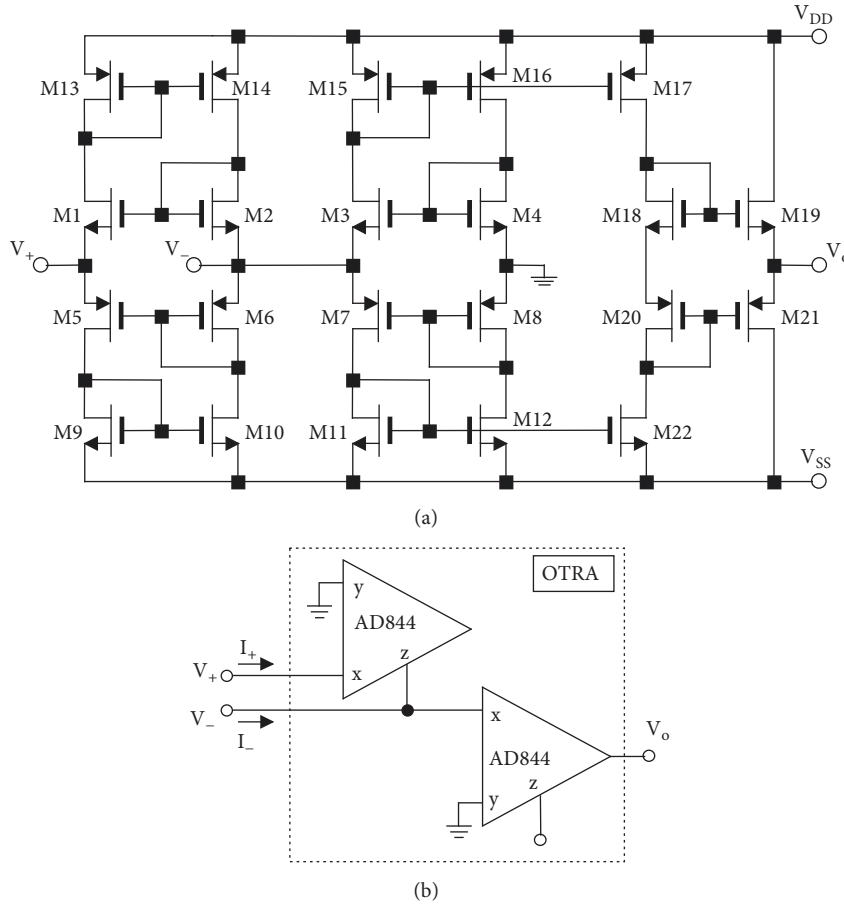

Figure 2: OTRA implementation based on (a) CMOS transistor-level and (b) integrated circuits (AD844s).

in a single-circuit scheme by arranging the switch (S) to connect at different terminals; and (4) the amplitude of the rectified output signal can be adjusted by tuning the bias voltages (V_a and V_b). Because the proposed rectifiers feature compact circuit topologies and this paper is the first report to present full-phase operation transresistance-mode precision full-wave rectifiers by using OTRAs, the proposed circuits can find many applications in development of industry circuit systems like high-performance power supplies, RF demodulators, AC voltmeters, and watt meters.

$$R = \frac{1}{\mu_n C_{ox} (W/L)_{M_A,M_B} (V_a - V_b)} \tag{4}$$

V_o (mode 1)

$$= \begin{cases} \dfrac{I_{in}}{\mu_n C_{ox} (W/L)_{M_A,M_B} (V_a - V_b)} & (I_{in} > 0) \\ \dfrac{-I_{in}}{\mu_n C_{ox} (W/L)_{M_A,M_B} (V_a - V_b)} & (I_{in} < 0) \end{cases} \tag{5}$$

V_o (mode 2)

$$= \begin{cases} \dfrac{-I_{in}}{\mu_n C_{ox} (W/L)_{M_A,M_B} (V_a - V_b)} & (I_{in} > 0) \\ \dfrac{I_{in}}{\mu_n C_{ox} (W/L)_{M_A,M_B} (V_a - V_b)} & (I_{in} < 0) \end{cases} \tag{6}$$

3. Nonideality Effects and Analyses

This section investigates the influences of the nonideal effects on the proposed circuits. Figure 5 presents a sophisticated equivalent circuit model of the applied OTRA (Figure 2(b)) [27]. According to the datasheet of AD844 [28], a practical AD844 can be modeled as a positive current conveyor (CC) cascading a voltage buffer (VBF) with parasitic resistances at terminals. In Figure 5, the resistances R_x and R_z represent the finite series and parallel parasitic resistances at x and z terminals of AD844. The series parasitic resistance R_x at x terminal is in the order of several tens of ohms, whereas the parallel parasitic input R_z is in the order of a few megaohms. Typical values of these parasitic resistances are $R_x = 50\ \Omega$ and $R_z = 3\ M\Omega$ [28]. However, in the ideal case, R_x is zero and R_z is treated as infinite. By applying the equivalent circuit model

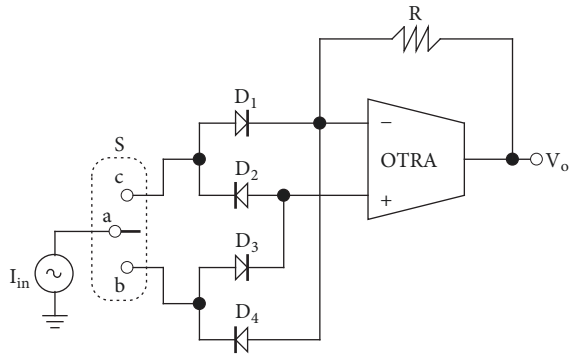

(a)

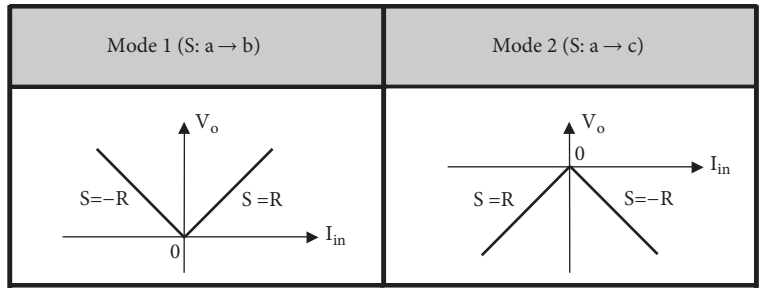

(b)

Figure 3: The proposed full-phase operation transresistance-mode precision full-wave rectifier: (a) circuit diagram and (b) input and output transfer characteristics.

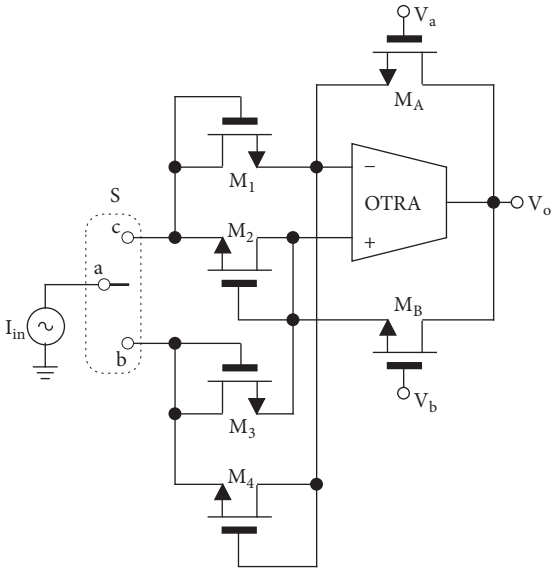

Figure 4: The proposed full MOSFET-based full-phase operation transresistance-mode precision full-wave rectifier.

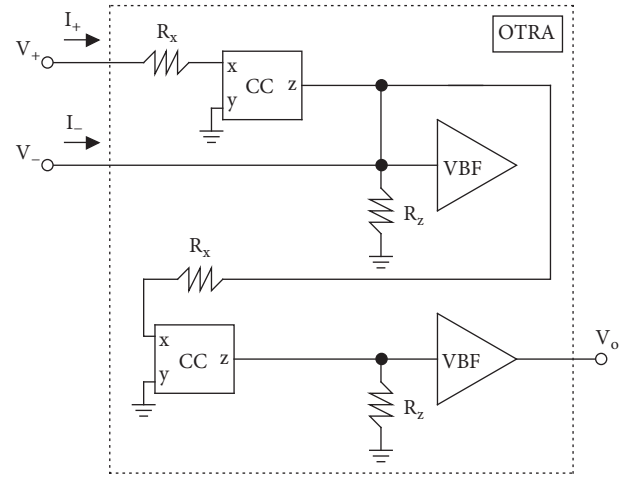

Figure 5: Equivalent circuit model of the OTRA (Figure 2(b)) with parasitic effects.

(Figure 5) to the circuits (Figures 3 and 4) and repeating the analysis steps presented in Section 2, (2), (3), (5), and (6) can be modified to (7), (8), (9), and (10). Equations (7), (8), (9), and (10) indicate that the parasitic resistances R_x and R_z slightly affected the input and output transfer characteristics of the circuits (Figures 3 and 4) to deviate from the analyzed results of the ideal scenario. The following conditions $R \gg R_x$, $R_z \gg R_x$, and $R_z \gg 1\,\Omega$ must be satisfied in the design procedure to minimize the influence of these parasitic effects on the circuits.

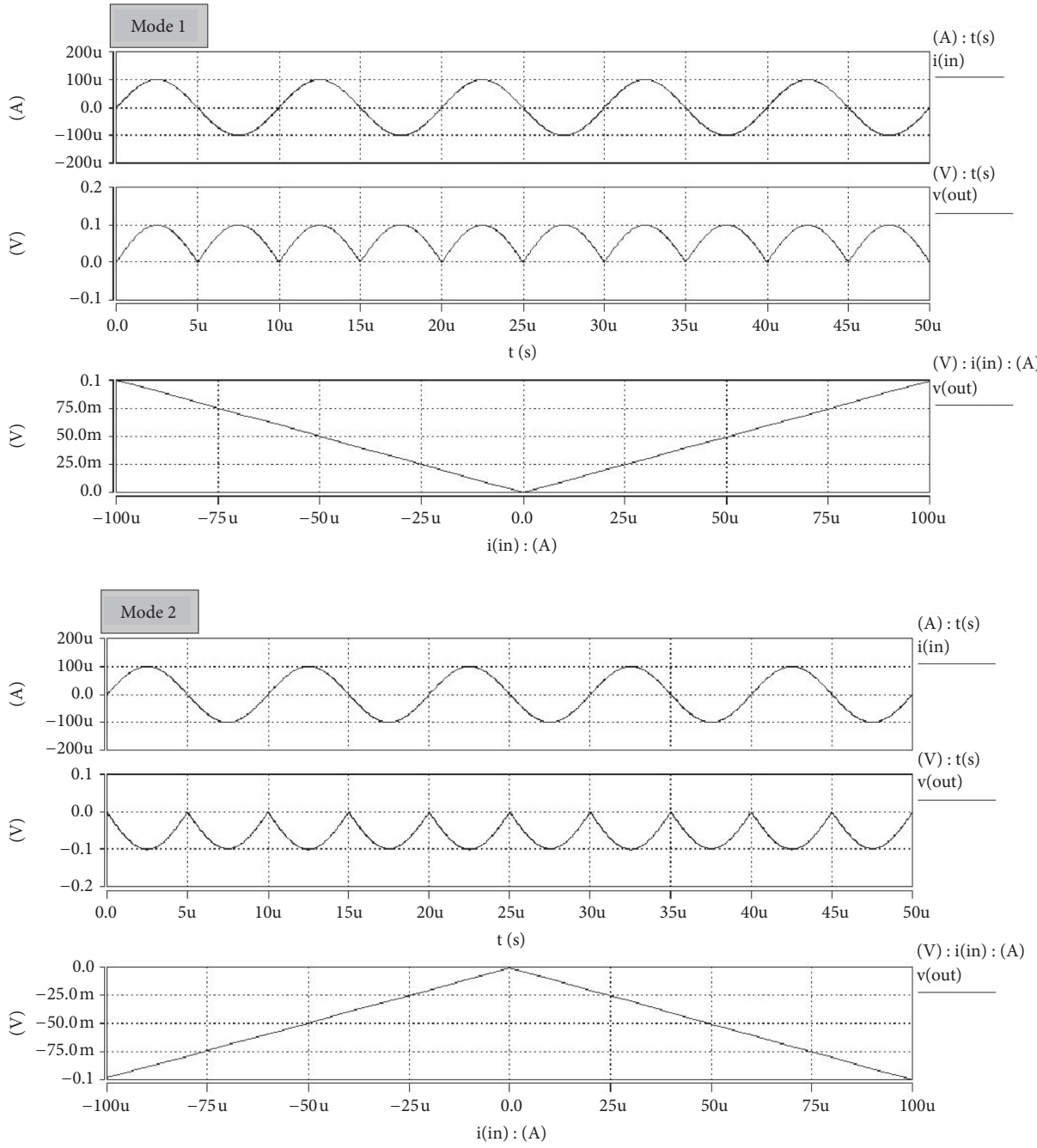

Figure 6: Simulation results of the input and rectified output waveforms and the corresponding input and output transfer characteristics of the circuit (Figure 3).

$$V_o \text{ (mode 1)} = \begin{cases} \dfrac{I_{in}}{1/R + 1/R_z - (R_x /\!/ R_z) / [R + (R_x /\!/ R_z)]\, R - (R_x /\!/ R_z) / [R + (R_x /\!/ R_z)]\, R_z} & (I_{in} > 0) \\ \dfrac{-I_{in}}{1/R + 1/R_z - (R_x /\!/ R_z) / [R + (R_x /\!/ R_z)]\, R - (R_x /\!/ R_z) / [R + (R_x /\!/ R_z)]\, R_z} & (I_{in} < 0) \end{cases} \tag{7}$$

$$V_o \text{ (mode 2)} = \begin{cases} \dfrac{-I_{in}}{1/R + 1/R_z - (R_x /\!/ R_z) / [R + (R_x /\!/ R_z)]\, R - (R_x /\!/ R_z) / [R + (R_x /\!/ R_z)]\, R_z} & (I_{in} > 0) \\ \dfrac{I_{in}}{1/R + 1/R_z - (R_x /\!/ R_z) / [R + (R_x /\!/ R_z)]\, R - (R_x /\!/ R_z) / [R + (R_x /\!/ R_z)]\, R_z} & (I_{in} < 0) \end{cases} \tag{8}$$

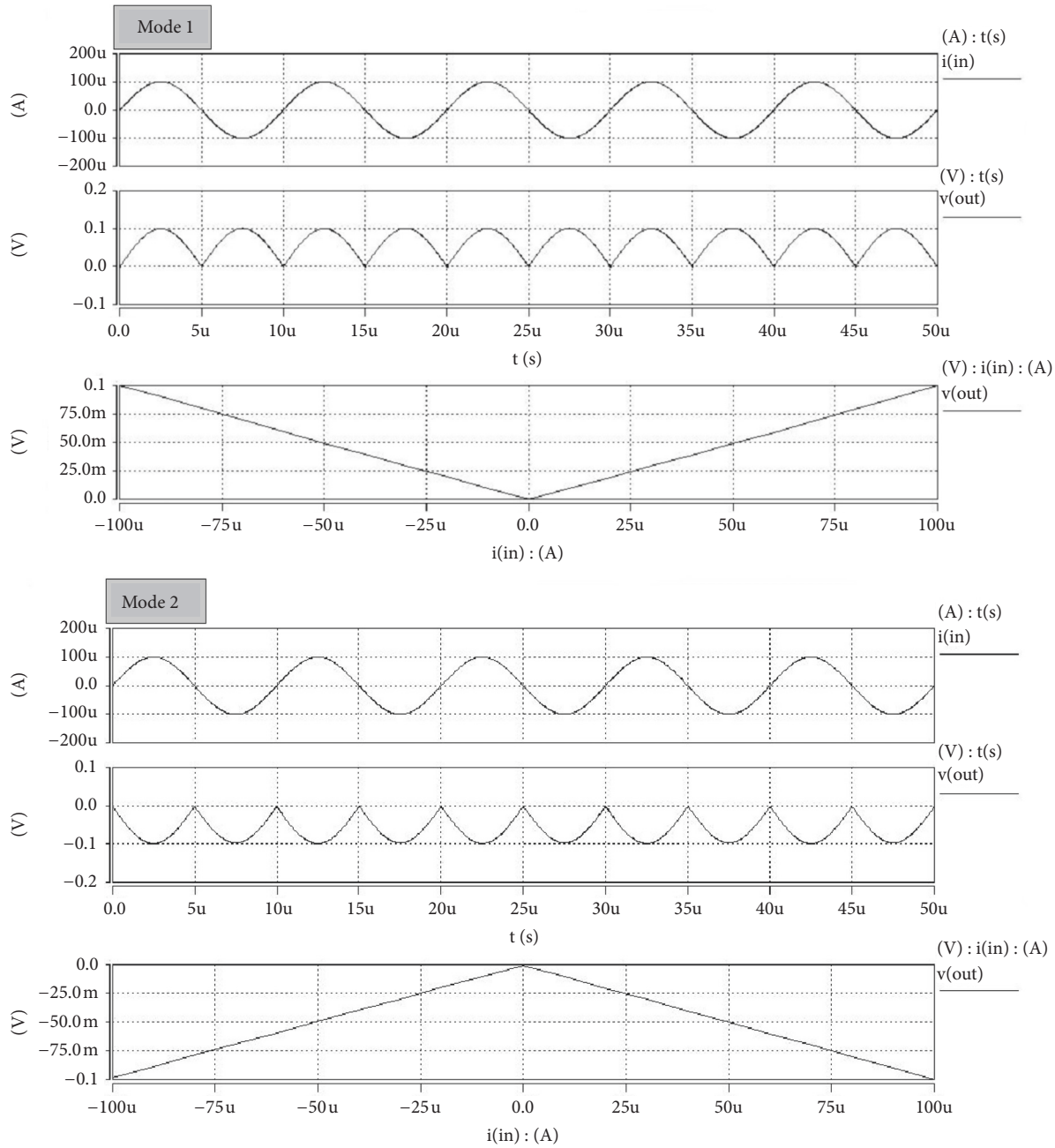

Figure 7: Simulation results of the input and rectified output waveforms and the corresponding input and output transfer characteristics of the circuit (Figure 4).

$$V_o \text{ (mode 1)} = \begin{cases} \dfrac{I_{in}}{\mu_n C_{ox}(W/L)_{M_A,M_B}(V_a - V_b) - \left((R_x /\!\!/ R_z)/\left(\left[\mu_n C_{ox}(W/L)_{M_A,M_B}(V_a - V_b)\right]^{-1} + (R_x /\!\!/ R_z)\right)\right)\left[\mu_n C_{ox}(W/L)_{M_A,M_B}(V_a - V_b) + 1/R_z\right] + 1/R_z} & (I_{in} > 0) \\ \dfrac{-I_{in}}{\mu_n C_{ox}(W/L)_{M_A,M_B}(V_a - V_b) - \left((R_x /\!\!/ R_z)/\left(\left[\mu_n C_{ox}(W/L)_{M_A,M_B}(V_a - V_b)\right]^{-1} + (R_x /\!\!/ R_z)\right)\right)\left[\mu_n C_{ox}(W/L)_{M_A,M_B}(V_a - V_b) + 1/R_z\right] + 1/R_z} & (I_{in} < 0) \end{cases} \quad (9)$$

$$V_o \text{ (mode 1)} = \begin{cases} \dfrac{-I_{in}}{\mu_n C_{ox}(W/L)_{M_A,M_B}(V_a - V_b) - \left((R_x /\!\!/ R_z)/\left(\left[\mu_n C_{ox}(W/L)_{M_A,M_B}(V_a - V_b)\right]^{-1} + (R_x /\!\!/ R_z)\right)\right)\left[\mu_n C_{ox}(W/L)_{M_A,M_B}(V_a - V_b) + 1/R_z\right] + 1/R_z} & (I_{in} > 0) \\ \dfrac{I_{in}}{\mu_n C_{ox}(W/L)_{M_A,M_B}(V_a - V_b) - \left((R_x /\!\!/ R_z)/\left(\left[\mu_n C_{ox}(W/L)_{M_A,M_B}(V_a - V_b)\right]^{-1} + (R_x /\!\!/ R_z)\right)\right)\left[\mu_n C_{ox}(W/L)_{M_A,M_B}(V_a - V_b) + 1/R_z\right] + 1/R_z} & (I_{in} < 0) \end{cases} \quad (10)$$

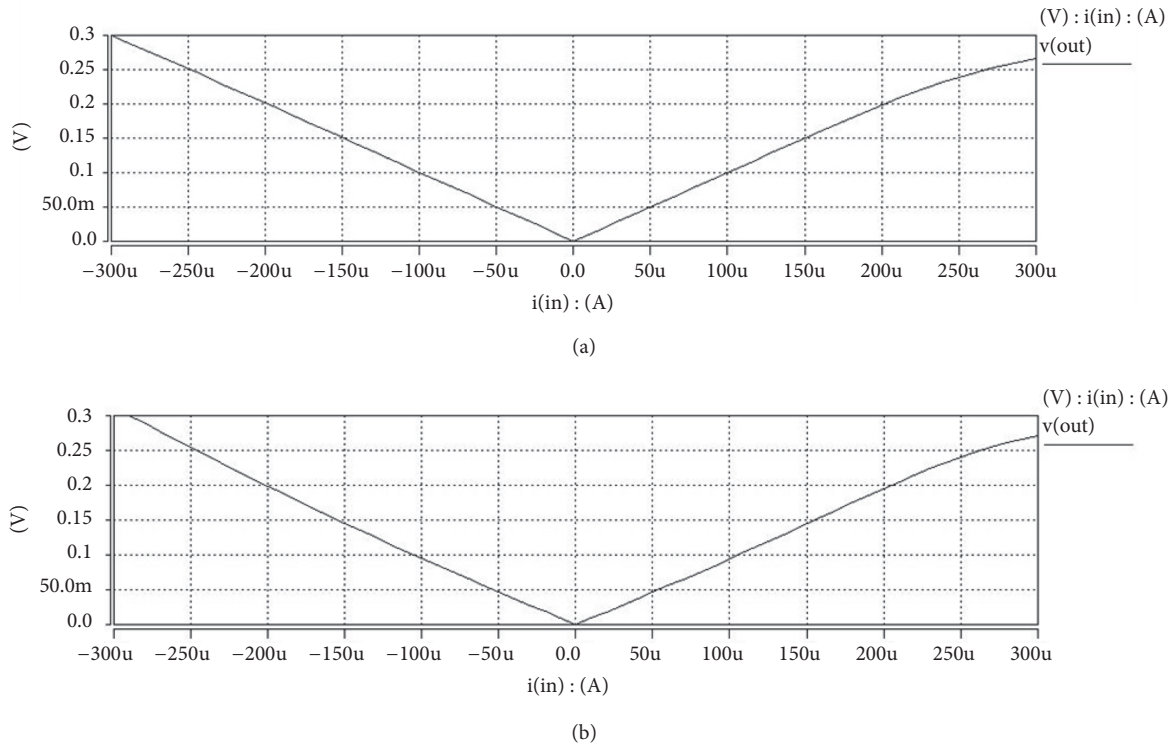

Figure 8: Simulation results of the input and output transfer characteristics in a wide scope of the (a) circuit in Figure 3 and (b) circuit in Figure 4.

4. Computer Simulations and Experimental Results

In this section, several simulations and experimental examples were conducted to verify the validity of the proposed circuits. The circuits (Figures 3 and 4) were simulated using HSPICE program based on the CMOS implementation of the OTRA (Figure 2(a)) by using the TSMC 0.25 μm CMOS process parameters. The aspect ratio of all MOS transistors of the OTRA (Figure 2(a)) and the MOS diodes (M_1–M_4; Figure 4) is W/L = 22 μm/2.2 μm. For the circuit (Figure 3), the diodes (D_1–D_4) used in simulation tests were constructed based on 1N914 diode model [29]. The supply voltages of the circuit (Figure 2(a)) used were $V_{DD} = -V_{SS} = 2.5$ V. In the first example, a sinusoidal signal with an amplitude of 100 μA and frequency of 100 kHz was applied to the input current (I_{in}) of the circuits (Figures 3 and 4). For the circuit (Figure 4), the resistor R = 1 kΩ was determined on the basis of (4) by setting the following circuit parameters: $(W/L)_{MA,MB}$ = 10 μm/2 μm, V_a = 1.76 V, and V_b = 0.5 V. Figures 6 and 7 display the simulation results of the time waveforms and the corresponding input and output transfer characteristics of the circuit under two diverse rectification output modes. The total power consumption was 2.31 mW. The simulation results were consistent with the theoretical predictions and confirmed that the circuits (Figures 3 and 4) performed a full-phase operation transresistance-mode full-wave rectification function in a single-circuit scheme.

The input and output transfer characteristics of the circuits (Figures 3 and 4) in the wide sweeping range of the input signal are displayed in Figure 8. Simulation results, obtained at a frequency of 1 MHz and by applying an input signal with amplitude of 100 μA, revealed that the circuits maintained a high degree of linearity in amplitude for the input current signal ranging from 0 to 250 μA. In Figure 8(a), the offset at zero crossing is determined as 586.34 μV, whereas in Figure 8(b), the offset at zero crossing is 577.27 μV.

To determine the minimal applicable amplitude of the input signal for the circuit (Figure 4), the circuit was arranged at frequencies of 1 Hz, 100 kHz, and 1 MHz and input current signals with diverse amplitudes of 80 and 50 μA were applied. The simulation results are presented in Figure 9 and indicated that the circuit reduced the amplitude of the rectified output to a low input signal amplitude. However, in the simulation tests, the circuit did not operate favorably when the amplitude of the input signal was lower than 10 μA.

To determine the applicable operating frequency range of the proposed precision rectifiers, the circuit (Figure 4) was used. The simulation results (Figure 10) obtained by applying an input current signal I_{in} = 100 μA and frequencies of 1 Hz, 1 MHz, and 5 MHz revealed that when the frequency of the input current signal was increased to 5 MHz, a rectified output with distortion was obtained from the circuit. The simulation results confirmed that the highest operating frequency of the circuit is limited at 5 MHz and thus the circuit can process an input signal at frequencies ranging

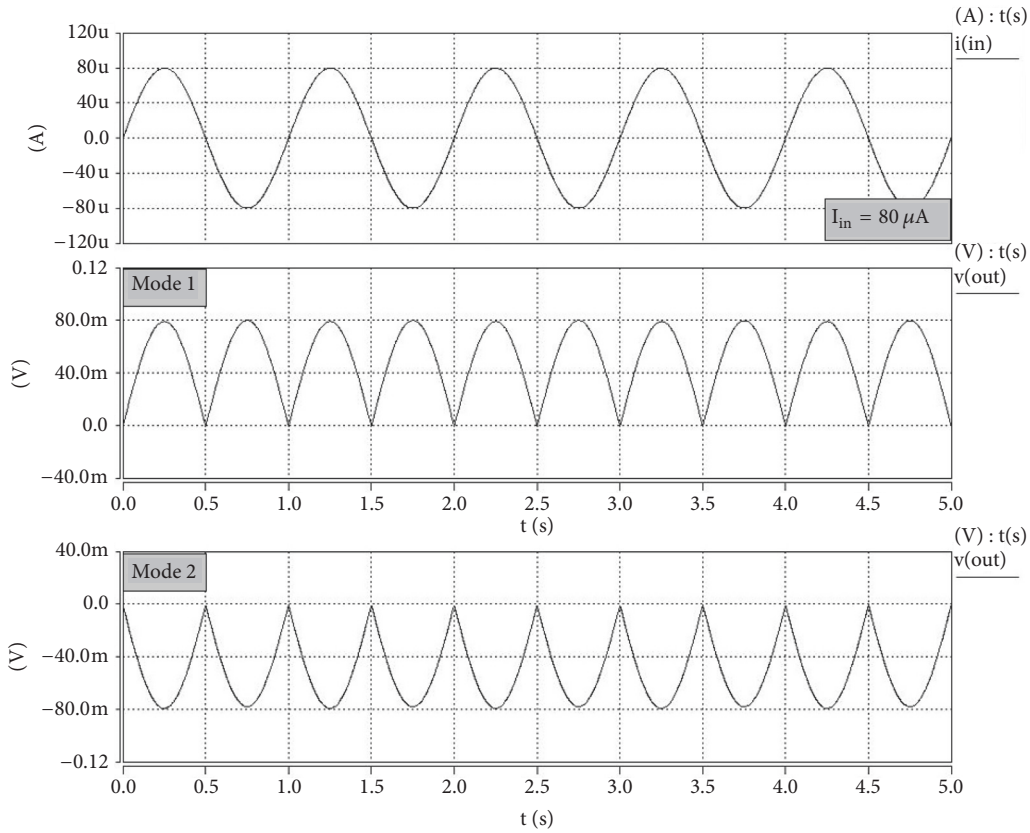

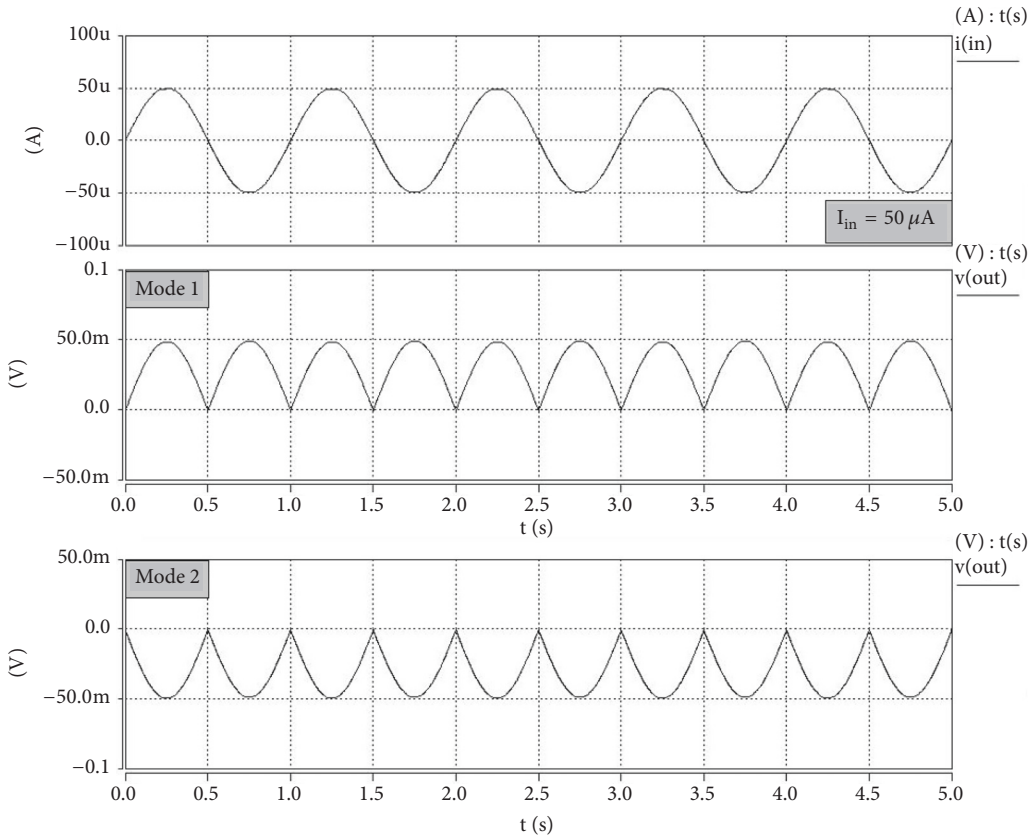

(a)

Figure 9: Continued.

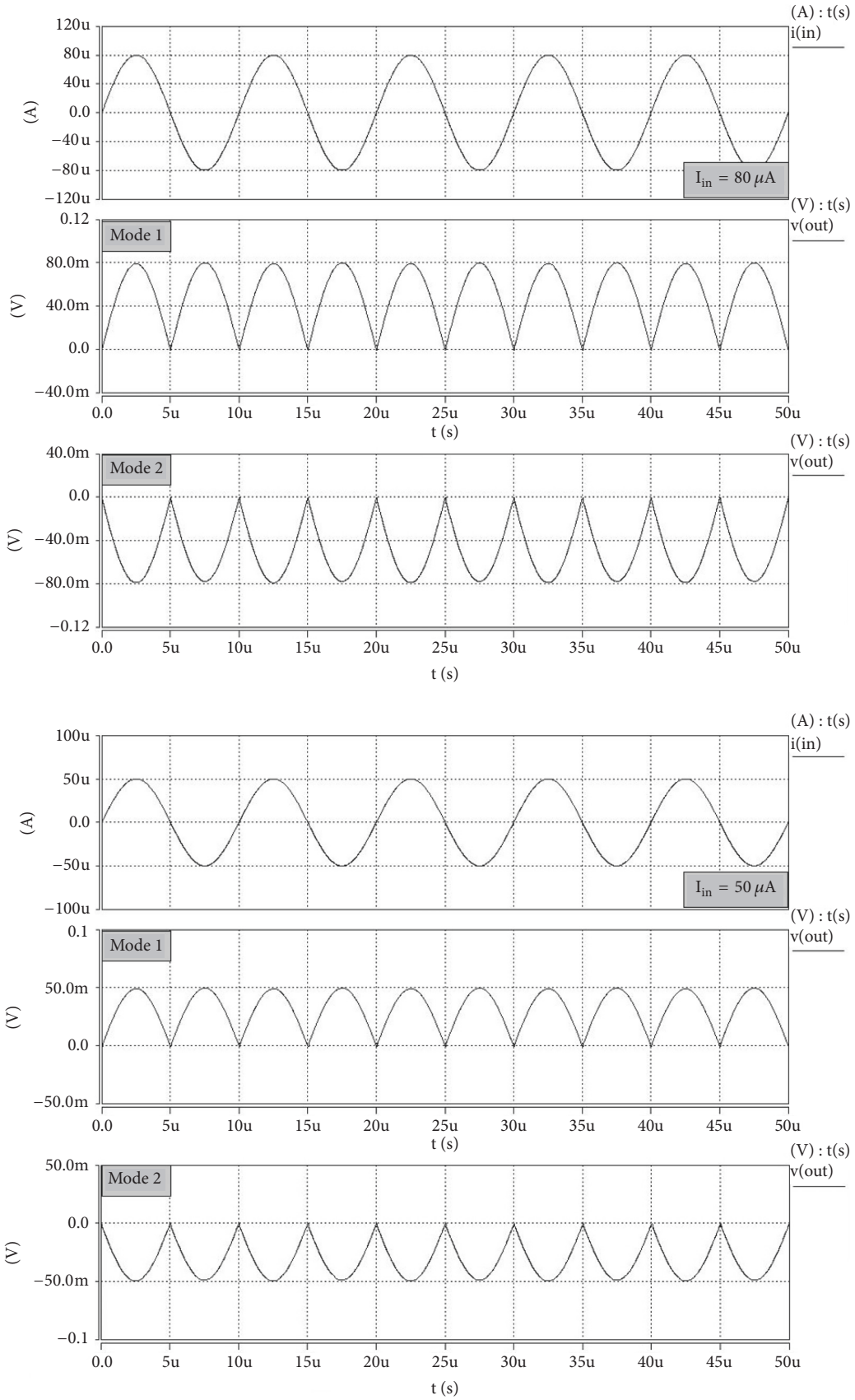

(b)

Figure 9: Continued.

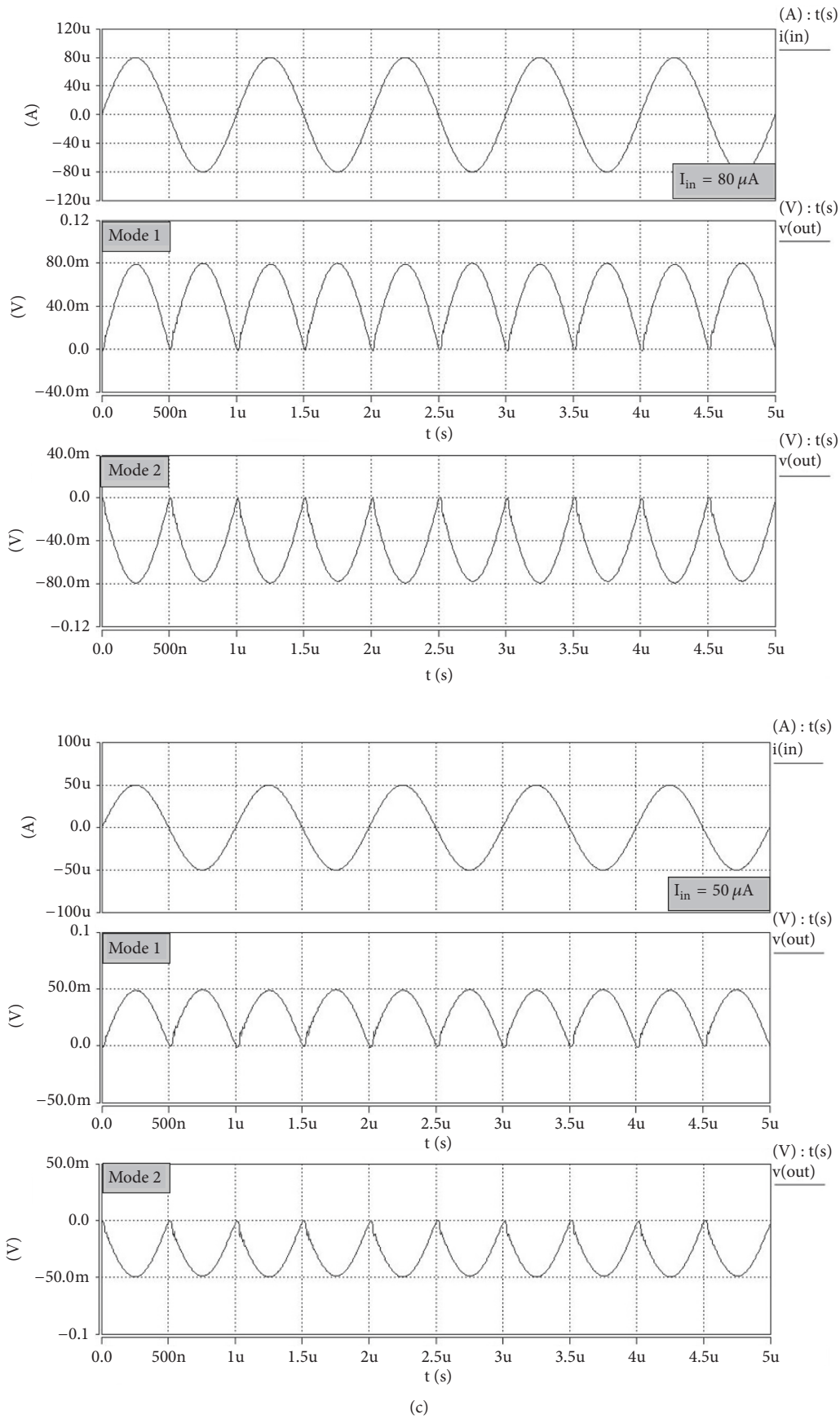

(c)

Figure 9: Simulation results of the input and rectified output waveforms of the circuit (Figure 4) at frequencies of (a) 1 Hz, (b) 100 kHz, and (c) 1 MHz for various input signal amplitudes.

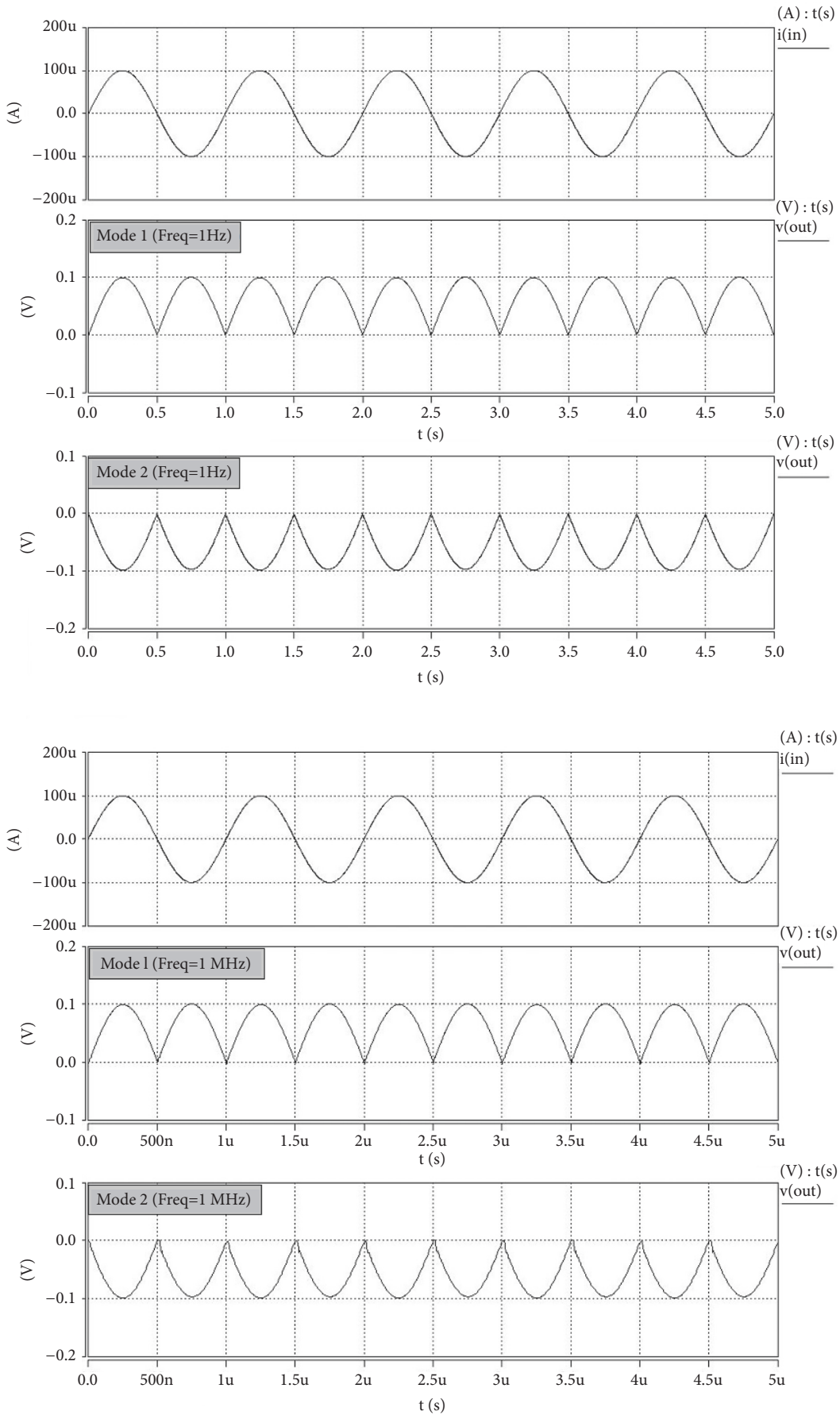

Figure 10: Continued.

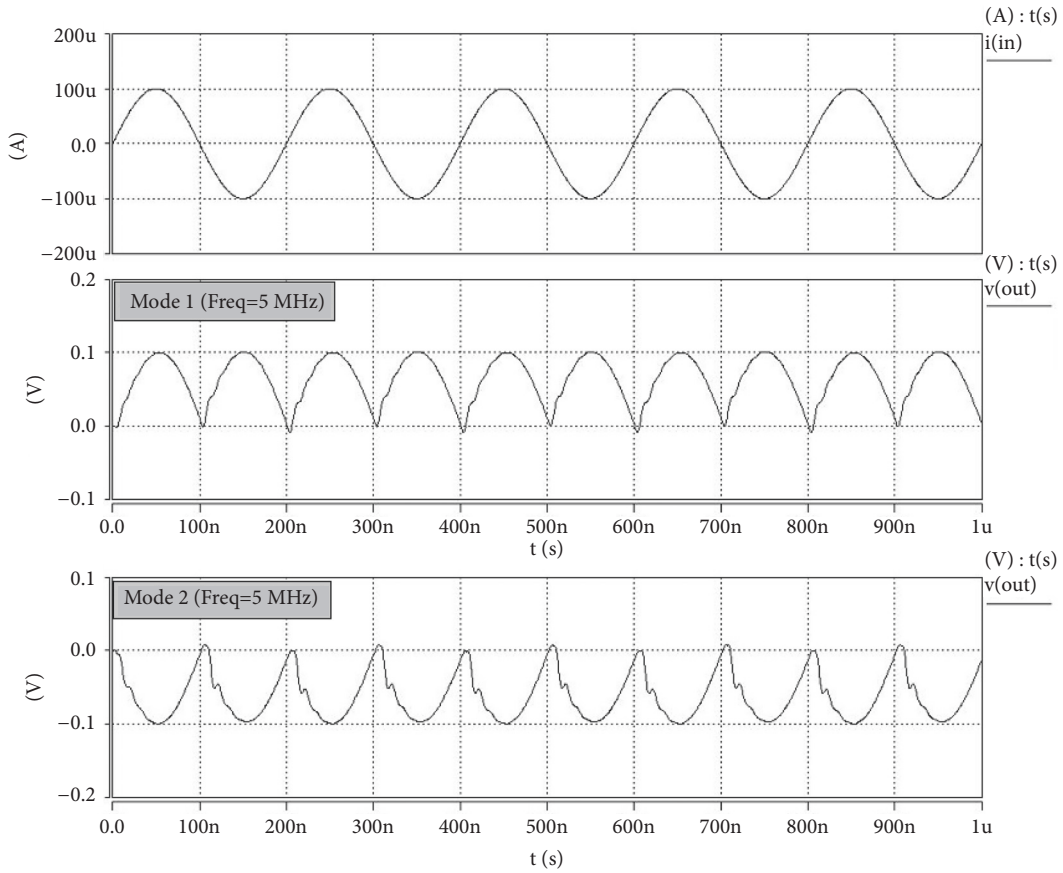

Figure 10: Simulation results of the input and rectified output waveforms of the circuit (Figure 4) at various frequencies for an input signal with an amplitude of 100 μA.

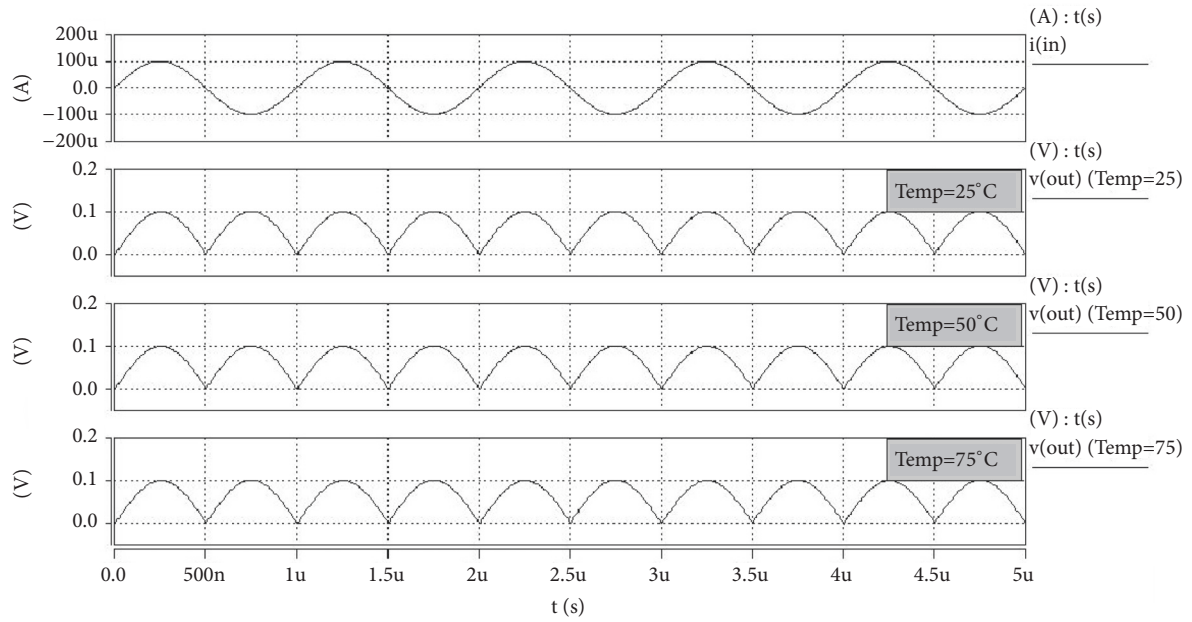

Figure 11: Simulation results of the input and rectified output waveforms of the circuit (Figure 3) under different temperature conditions.

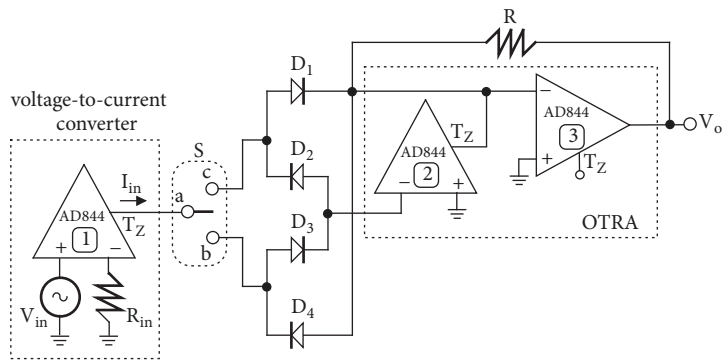

Figure 12: Complete hardware implementation of the circuit (Figure 3) for conducting the experiments.

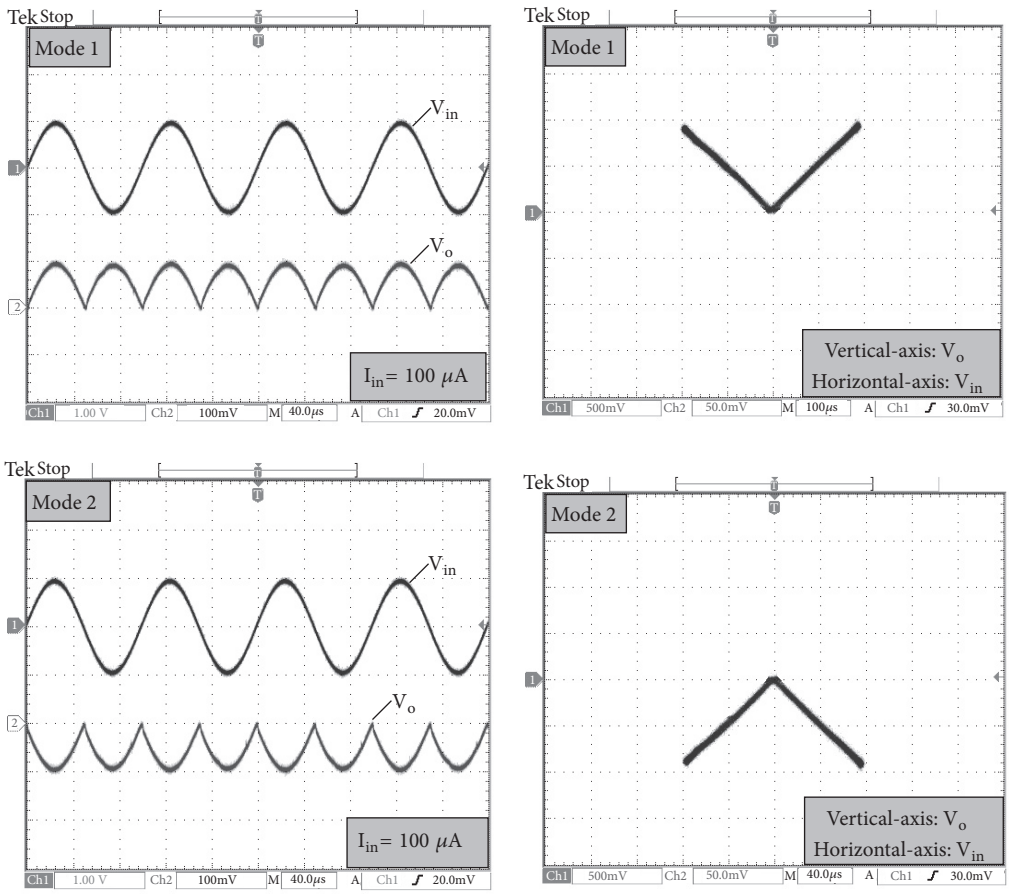

Figure 13: Experimental results of the input and rectified output waveforms and the corresponding input and output transfer characteristics of the circuit (Figure 3).

from several hertz to several megahertz. It should be noted that the highest applicable operating frequency limited of the proposed rectifiers depends on the distortion at zero crossing owing to the maximum slew-rate of the output voltage for the active device and turn-on and turn-off transition of diodes and MOSFETs. However, a high slew-rate OTRA and high-speed diodes can be used to extend a higher operating frequency.

With regard to the temperature stabilities of the proposed rectifiers, the circuit (Figure 3) was used. Simulation tests were performed at frequency of 1 MHz and input current signal with amplitude of 100 μA at different temperatures over a 25°C to 75°C range. Simulation results were recorded in Figure 11 and showed that the output amplitude deviations between the theoretical values and the simulated results are below 1%.

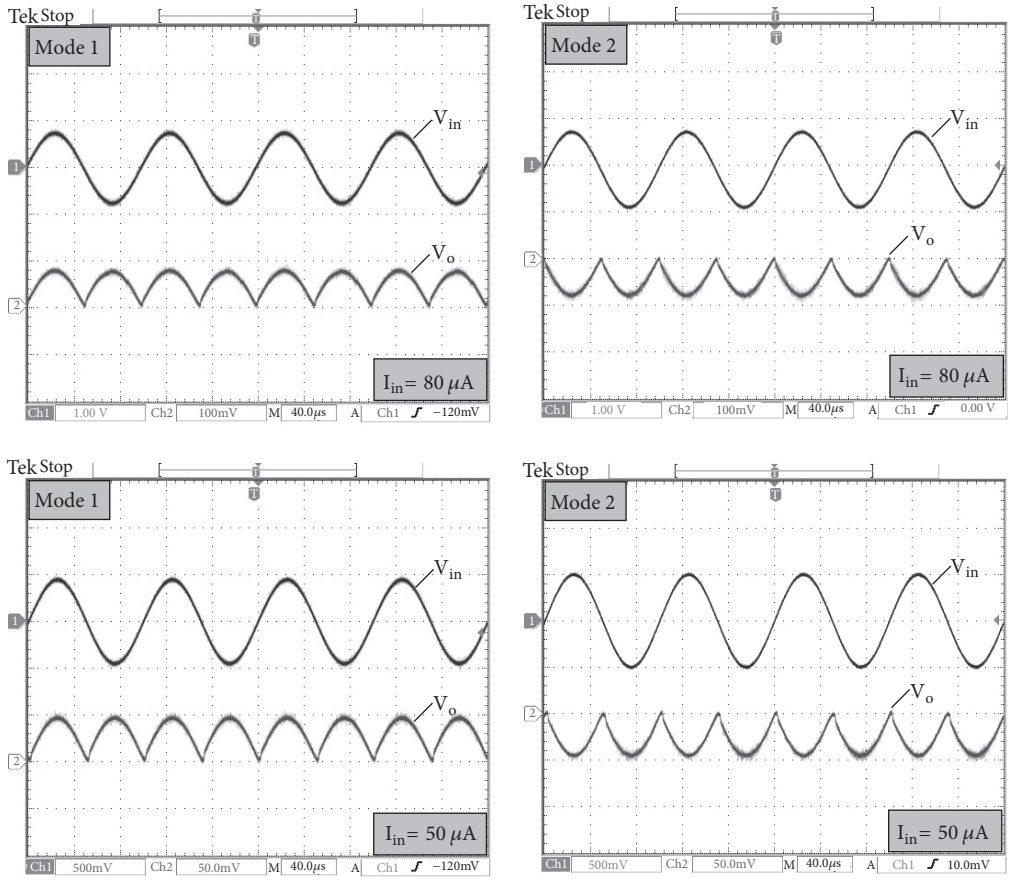

Figure 14: Experimental results of the input and rectified output waveforms of the circuit (Figure 3) for various input signal amplitudes.

In addition to the circuit simulations, a prototype of the circuit (Figure 3) was implemented to conduct experiments using the AD844 integrated circuits (Figure 2(b)) and discrete passive components. The complete hardware implementation of the circuit (Figure 3) for conducting the experiments is presented in Figure 12. In Figure 12, the first AD844 combined with the grounded resistor R_{in} functions as a voltage-to-current converter [30], which was used to produce an input current signal (I_{in}) as shown in Figure 3. From Figure 12 and according to the terminal behaviors of an AD844 [28], the relationship between I_{in} and V_{in} can be determined as $I_{in} = V_{in}/R_{in}$. All experiments were performed at supply voltages of ±3.5 V. In the experiment, 1N914 diodes (D_1–D_4) were adopted and the switch (S) was implemented by utilizing commercially available single-pole double-throw switch. Several experiments were conducted as follows.

To determine whether the circuit (Figure 3) performed full-phase operation full-wave rectification in a single-circuit scheme, a sinusoidal signal with an amplitude and a frequency of 100 μA and 10 kHz, respectively, was applied to the input I_{in} of the circuit (Figure 3). To obtain an amplitude of the input current signal (I_{in}) of 100 μA, a voltage sinusoidal signal (V_{in}) with an amplitude of 1 V and R_{in} = 10 kΩ was applied (Figure 12). Figure 13 presents the experimental results of the circuit (Figure 3) that was operated in two diverse full-wave rectified output modes. In this experiment, the value of the resistor R was selected as 1 kΩ. To investigate the minimal applicable amplitude of the input signal for the circuit (Figure 3), the following experiments were conducted. First, the resistors R = 1 kΩ and R_{in} = 10 kΩ were selected. Next, the input current signal I_{in} with a frequency of 10 kHz at distinct amplitudes of 80 μA (V_{in} = 0.8 V) and 50 μA (V_{in} = 0.5 V) was applied to record the rectified output waveforms. Figure 14 presents the time waveforms at various amplitudes. However, the circuit did not operate favorably when the amplitude of the input current signal (I_{in}) was lower than 30 μA in the experimental tests. These experimental results indicated that the minimal applicable amplitude of the input signal for the circuit (Figure 3) was limited to several tens of micro amperes based on the OTRA (Figure 2(b)) constructed using the commercially integrated circuits (AD844s) on a breadboard. One feature of the proposed circuits (Figures 3 and 4) is that the resistor R can be used to adjust the amplitude of the rectified output waveform. Two test results with the rectified output waveforms of V_o = 50 mV (R = 0.5 kΩ) and V_o = 200 mV (R = 2 kΩ) at a peak sinusoidal signal and frequency of I_{in} = 100 μA and 10 kHz, respectively, are shown in Figures 15 and 16.

For the circuit (Figure 4), the resistor R was determined on the basis of (4) by setting the following parameters: R = 0.5 kΩ (V_a = 3.1 V and V_b = 0.5 V) and R = 2 kΩ (V_a = 1.2 V and V_b = 0.5 V). Simulation and experimental results

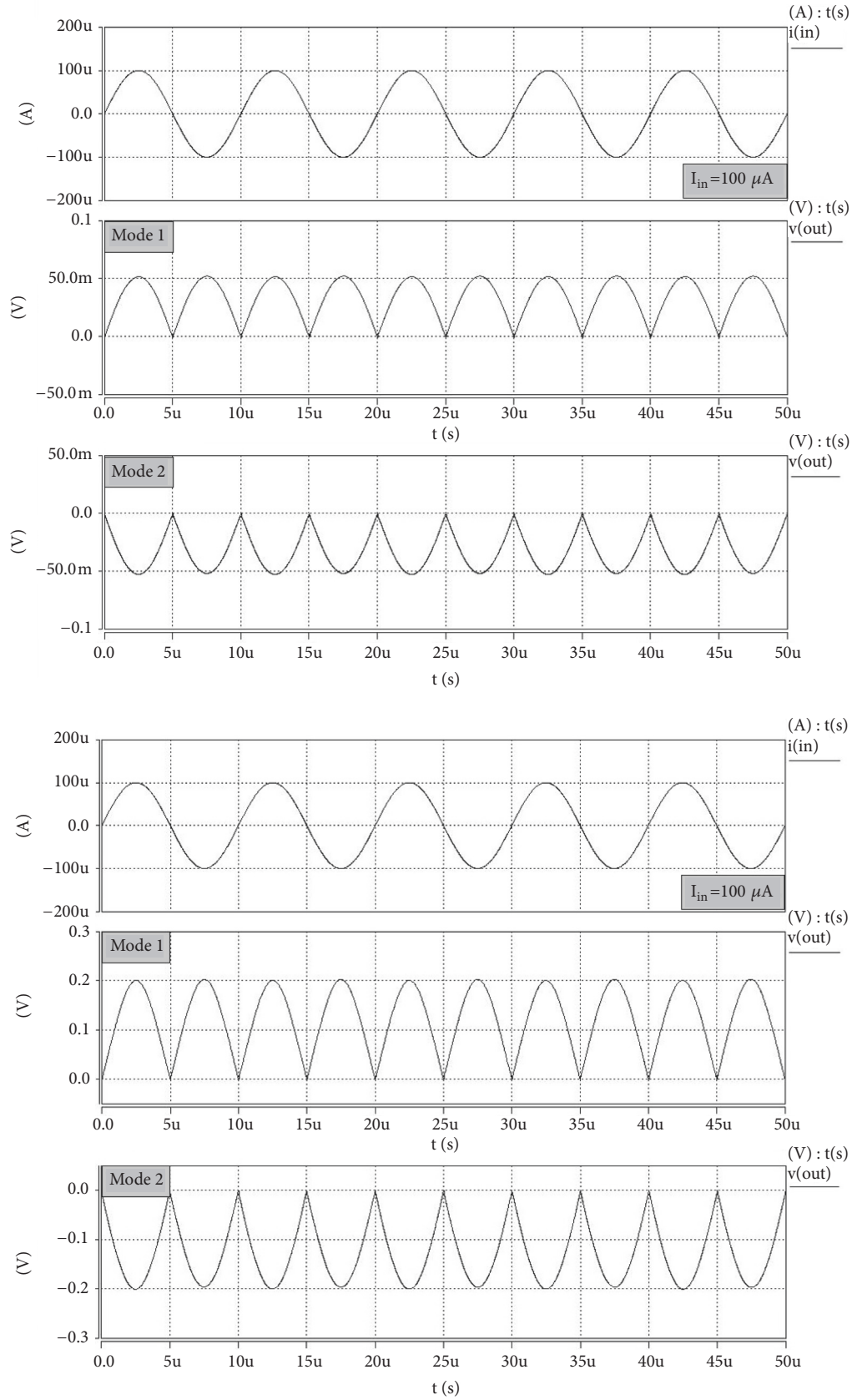

Figure 15: Simulation results of the tunable rectified output amplitude for the circuit (Figure 4).

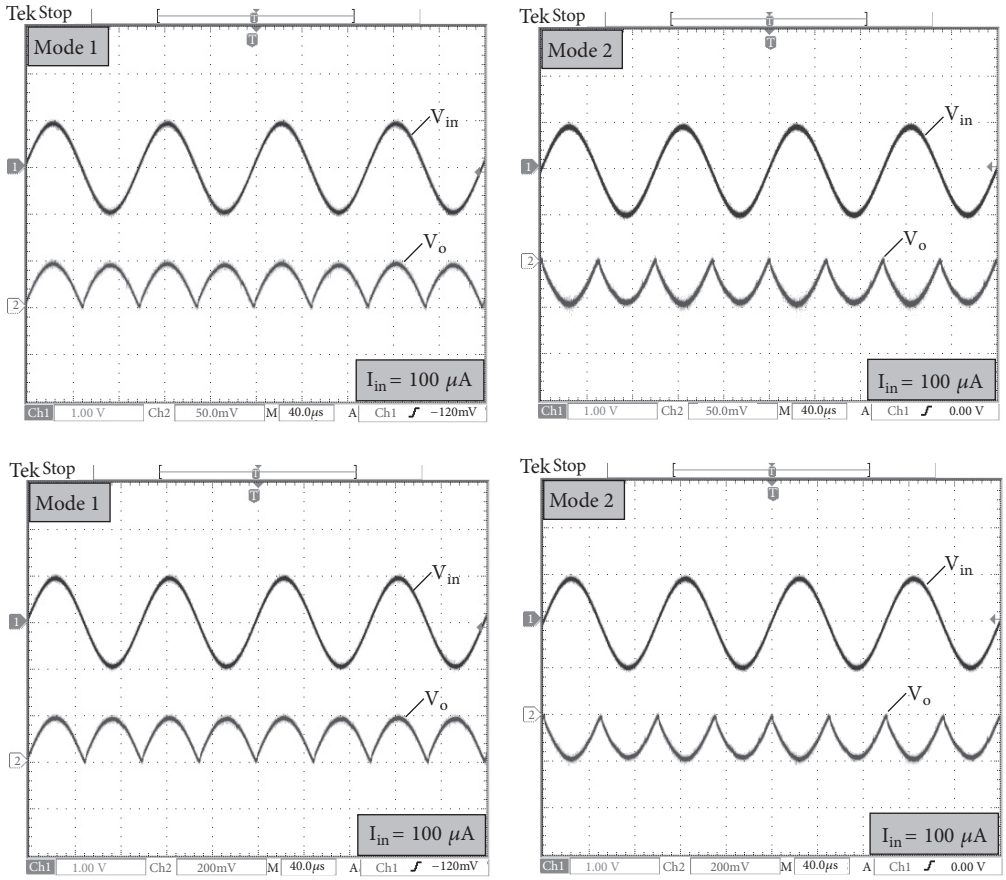

Figure 16: Experimental results of the tunable rectified output amplitude for the circuit (Figure 3).

indicated that the amplitude of the rectified output signal was tunable by varying the resistor R. The maximum slew-rate of the AD844 and the highest applicable operating frequency of the diodes constitute the main obstacle to obtaining the highest applicable frequency in the circuit (Figure 12). The highest applicable operating frequency of the prototype circuit (Figure 12) was limited at approximately 200 kHz in the experimental tests. For comparison, the limited high-speed application of other full-wave rectifiers in Table 1 was also given. The simulation and experimental results supported the theoretical analyses, confirming the feasibility of the proposed circuits.

5. Conclusions

This study presented two designs of OTRA-based full-phase operation transresistance-mode precision full-wave rectifiers. Unlike the previously OTRA-based voltage-mode precision rectifiers, the proposed designs belong to transresistance-mode rectification solutions. Computer simulations and experimental results were presented to validate the efficiency of the circuits, which were consistent with the theoretical analyses. Thus, this study sparks a beginning for research into transresistance-mode precision rectifier design and can provide new possibilities for OTRA device application in current analog signal processing systems.

Data Availability

No data were used to support this study.

Conflicts of Interest

The author declares that there are no conflicts of interest regarding the publication of this article.

References

[1] S. Franco, *Design with Operational Amplifiers and Analog Integrated Circuits*, McGraw-Hall, New York, NY, USA, 2001.

[2] C. Toumazou, F. J. Lidgey, and S. Chattong, "High frequency current conveyor precision full-wave rectifier," *IEEE Electronics Letters*, vol. 30, no. 10, pp. 745-746, 1994.

[3] A. A. Khan, M. Abou El-Ela, and M. A. Al-Turaigi, "Current-mode precision rectification," *International Journal of Electronics*, vol. 79, no. 6, pp. 853–859, 1995.

[4] B. Wilson and V. Mannama, "Current-mode rectifier with improved precision," *IEEE Electronics Letters*, vol. 31, no. 4, pp. 247-248, 1995.

[5] W. Surakampontorn, K. Anuntahirunrat, and V. Riewruja, "Sinusoidal frequency doubler and full-wave rectifier using translinear current conveyor," *IEEE Electronics Letters*, vol. 34, no. 22, pp. 2077–2079, 1998.

[6] A. Monpapassorn, "Low output impedance dual CCII full-wave rectifier," *International Journal of Electronics*, vol. 100, no. 5, pp. 648–654, 2013.

[7] E. Yuce, S. Minaei, and O. Cicekoglu, "Full-wave rectifier realization using only two CCII+s and NMOS transistors," *International Journal of Electronics*, vol. 93, no. 8, pp. 533–541, 2006.

[8] S. Minaei and E. Yuce, "A new full-wave rectifier circuit employing single dual-X current conveyor," *International Journal of Electronics*, vol. 95, no. 8, pp. 777–784, 2008.

[9] E. Sánchez-Sinencio, J. Ramírez-Angulo, B. Linares-Barranco, and A. Rodríguez-Vízquez, "Operational transconductance amplifier-based nonlinear function syntheses," *IEEE Journal of Solid-State Circuits*, vol. 24, no. 6, pp. 1576–1586, 1989.

[10] M. Kumngern and K. Dejhan, "High frequency and high precision CMOS full-wave rectifier," *International Journal of Electronics*, vol. 93, no. 3, pp. 185–199, 2006.

[11] C. Jongkunstidchai, C. Fongsamut, K. Kumwachara, and W. Surakampontorn, "Full-wave rectifiers based on operational transconductance amplifiers," *AEÜ - International Journal of Electronics and Communications*, vol. 61, no. 3, pp. 195–201, 2007.

[12] M. Sagbas, S. Minaei, and U. E. Ayten, "Component reduced current-mode full-wave rectifier circuits using single active component," *IET Circuits, Devices & Systems*, vol. 10, no. 1, pp. 1–11, 2016.

[13] W. Tangsrirat, T. Pukkalanun, and W. Surakampontorn, "Synthesis of current differencing transconductance amplifier-based current limiters and its applications," *Journal of Circuits, Systems and Computers*, vol. 20, no. 2, pp. 185–206, 2011.

[14] F. Khateb, J. Vávra, and D. Biolek, "A novel current-mode full-wave rectifier based on one CDTA and two diodes," *Radioengineering*, vol. 19, no. 3, pp. 437–445, 2010.

[15] N. Pandey and R. Pandey, "Current mode full-wave rectifier based on a single MZC-CDTA," *Active and Passive Electronic Components*, vol. 2013, Article ID 967057, 5 pages, 2013.

[16] D. Biolek, E. Hancioglu, and A. Ü. Keskin, "High-performance current differencing transconductance amplifier and its application in precision current-mode rectification," *AEÜ - International Journal of Electronics and Communications*, vol. 62, no. 2, pp. 92–96, 2008.

[17] K. Anuntahirunrat, W. Tangsrirat, V. Riewruja, and W. Surakampontorn, "Sinusoidal frequency doubler and full-wave rectifier based on translinear current-controlled current conveyors," *International Journal of Electronics*, vol. 91, no. 4, pp. 227–239, 2004.

[18] S. Maheshwari, "Current controlled precision rectifier circuits," *Journal of Circuits, Systems and Computers*, vol. 16, no. 1, pp. 129–138, 2007.

[19] J. Koton, N. Herencsar, and K. Vrba, "Minimal configuration precision full-wave rectifier using current and voltage conveyors," *IEICE Electronics Express*, vol. 7, no. 12, pp. 844–849, 2010.

[20] S. J. G. Gift and B. Maundy, "Versatile precision full-wave rectifiers for instrumentation and measurements," *IEEE Transactions on Instrumentation and Measurement*, vol. 56, no. 5, pp. 1703–1710, 2007.

[21] R. Anurag, N. Pandey, R. Pandey, and R. Vljay, "OTRA based precision rectifier," *I-Manager's Journal on Electronics Engineering*, vol. 6, no. 1, pp. 21–26, 2015.

[22] S. Oruganti, Y. Gilhotra, N. Pandey, and R. Pandey, "New topologies for OTRA based programmable precision half-wave and full-wave rectifiers," in *Proceedings of the 2017 Recent Developments in Control, Automation and Power Engineering, RDCAPE 2017*, pp. 327–331, Noida, India, October 2017.

[23] H.-C. Chien, "Switch-controllable full-phase operation precision half-wave rectifier using a single OTRA," *Journal of Circuits, Systems and Computers*, vol. 25, no. 7, 21 pages, 2016.

[24] J.-J. Chen, H.-W. Tsao, and C.-C. Chen, "Operational transresistance amplifier using CMOS technology," *IEEE Electronics Letters*, vol. 28, no. 22, pp. 2087-2088, 1992.

[25] C. Hou, H. Chien, and Y. Lo, "Squarewave generators employing OTRAs," *IEE Proceedings - Circuits, Devices and Systems*, vol. 152, no. 6, pp. 718–722, 2005.

[26] K. N. Salama and A. M. Soliman, "CMOS operational transresistance amplifier for analog signal processing," *Microelectronics Journal*, vol. 30, no. 3, pp. 235–245, 1999.

[27] Y. Lo, H. Chien, and H. Chiu, "Switch-controllable OTRA-based bistable multivibrators," *IET Circuits, Devices & Systems*, vol. 2, no. 4, pp. 373–382, 2008.

[28] "Analog devices AD844AN data sheet," http://www.alldatasheet.com/view.jsp?Searchword=Ad844%20datasheet&gclid=EAIaIQobChMI9ZTUhY7J4AIV06mWCh2_MgSaEAAYASAAEgKv8vD_BwE.

[29] "Fairchild semiconductor 1N914 data sheet," http://www.alldatasheet.com/view.jsp?Searchword=1n914%20datasheet&gclid=EAIaIQobChMIrJGUiY_J4AIVmamWCh0oMgFsEAAYASAAEgLeBvD_BwE.

[30] G. Ferri and N. C. Guerrini, *Low-Voltage Low-Power CMOS Current Conveyors*, Kluwer Academic Publishers, Boston, Mass, USA, 2003.